International Journal of Mass Spectrometry 304 (2011) 15–24

Contents lists available at ScienceDirect

International Journal of Mass Spectrometry

journal homepage: www.elsevier.com/locate/ijms

A combined theoretical and experimental study of mechanisms of fragmentation active for PHB oligomers in negative-ion mode multistage mass spectrometry

Henryk Bednarski[a,*], Karl Sohlberg[b], Marian Domański[a], Jan Weszka[a], Grażyna Adamus[a], Marek Kowalczuk[a], Vasile Cozan[c]

[a] Centre of Polymer and Carbon Materials, Polish Academy of Sciences, 34 M. Curie-Skłodowska Str., 41-819 Zabrze, Poland
[b] Department of Chemistry, Drexel University, 3141 Chestnut Street, Philadelphia, PA 19104, USA
[c] Petru Poni Institute of Macromolecular Chemistry, Aleea Gr. Ghica Voda 41 A, 700487 Iasi, Romania

ARTICLE INFO

Article history:
Received 8 October 2010
Received in revised form 14 February 2011
Accepted 1 March 2011
Available online 10 March 2011

Keywords:
CID
DFT
MD simulations
Polyhydroxyalkanoates

ABSTRACT

First-principles studies of the potential energy profiles for dissociation of poly[(R, S)-3-hydroxybutanoic acid] $[PHB_n\text{-}H]^-$ anions by proton rearrangement and direct fragmentation, as well as subsequent statistical RRKM analysis, indicate that fragmentation should proceed mainly through successive loss of a single 86 Da neutral unit (propene + CO_2). This theoretically predicted fragmentation mechanism is inconsistent with that proposed in the literature based on experiments, which suggests that proton rearrangements are the only active fragmentation channels in CID of $[PHB_n\text{-}H]^-$. We have combined experimental ESI-MS/MS fragmentation studies of $[PHB_n\text{-}H]^-$ with first-principles explorations of the potential energy surfaces, and molecular dynamics simulations of CID and thermal fragmentation events to understand this discordance. Both proton rearrangement and direct fragmentation channels are considered. The results reveal that the fragmentations observed at low collision energy favor the direct fragmentation channel and are more closely modeled as a thermal fragmentation process. By contrast, fragmentations observed at higher collision energy favor the indirect fragmentation channels and are more closely modeled as a fast CID process.

1. Introduction

Biodegradable polymers, including both naturally occurring biopolymers and synthetic mimics, form a group of polymeric materials of emerging importance. Polyhydroxyalkanoates (PHAs) belong to one of the most important and dynamically developing family of biopolymers [1–6]. Within this family more than 150 different monomers can be combined to give materials with an extremely wide range of properties [4]. High molecular weight natural poly[(R, S)-3-hydroxybutanoic acid] (PHB), is wide-spread in biological systems. It is produced by certain bacteria as a means of storing energy and carbon [5]. Synthetic analogues of natural PHB, obtained by ring-opening polymerization, posses various tacticities mimicking those found in nature [7,8].

Being biodegradable and biocompatible, thermoplastics of PHB have attracted industrial attention as environmentally degradable materials for a wide range of packaging, agricultural, marine and medical applications. Therefore, knowledge of the molecular structure of natural PHB as well as of its synthetic analogues is of great importance.

Mass spectrometry techniques enable gathering information on synthetic polymers complementary to that obtained by other techniques, e.g. gel permeation chromatography, light scattering, nuclear magnetic resonance spectroscopy and infrared spectroscopy. Matrix-assisted laser desorption/ionization (MALDI) and electrospray ionization (ESI) have been found to be the most convenient ionization techniques for the mass spectrometric analysis of polymers [9–12]. Due to the separation of the peaks corresponding to polyester chains of different lengths, the structures of the end groups and repeating units may be inferred from the fragment masses [9–19]. Additional insight into the structure of an individual polyester chain can be achieved with multistage mass spectrometry (MS^n), where the molecular ion of interest is separated from all other ions formed during ionization and induced to dissociate into fragments that can be used to decipher the chemical structure of the polyester end groups as well as the arrangements of co-monomer structural units along the copolyester chain. Sequencing data for individual macromolecular ions can be achieved by means of mass spectrometric fragmentation techniques such as collision induced dissociation (CID) and postsource decay (PSD). MS^n experiments may be performed in either positive or negative ion mode depend-

* Corresponding author. Tel.: +48 32 271 60 77.
E-mail address: hbednarski@cmpw-pan.edu.pl (H. Bednarski).

1387-3806/$ – see front matter © 2011 Elsevier B.V. All rights reserved.
doi:10.1016/j.ijms.2011.03.001

ing on the specific ionization technique used [9–26]. Cations are formed by complexation of the species studied with a positive ion such as (e.g., Na^+, K^+), whereas anion formation is based on proton removal, thus the ion studied differs in core chemical composition from neutral precursor species [9,10].

In addition to sequencing and structural information, mass spectrometry studies can provide insight into the mechanism of fragmentation. Previous fragmentation studies of individual molecular ions of such polyesters as: poly-3-hydroxybutyrate [14,15], poly[hydroxybutyrate-co-hydroxyvalerate] [13,17], poly(2-butyl-2ethyl-1,3-propylenephtalate) [20], poly(dipropoxylated bisphenol-A/adipic acid) [21], poly(2-methyl-3-hydroxyoctanoate) [16], poly[(R,S)-3-hydroxybutyrate-*co*-hydroxyhexanoate] [19], adipic acid/terephthalic acid/neopentyl glycol copolyesters [21,22], poly[butylene adipate] [23], poly[(R,S)-3-hydroxybutyrate-co-L-lactide) [24], poly(3-hydroxy-4-alkokxybutyrate) [25], and (R,S)-3-hydroxybutyrate/(R,S)-3-hydroxy-4-ethoxybutyrate copolyester [26] revealed that hydrogen rearrangement is typically present in the mechanism of fragmentation for those polyesters that dissociate by ester bond cleavage. More precisely, from the structures assigned, the end groups formed and the product ions present in MS^n spectra of the positive and negative ions selected from the polyesters studied, a β-hydrogen-transfer mechanism has been proposed [13,14,16,17,19,15,20–26]. The CH_2 (methylene) groups in PHB units exhibit increased acidity because they are activated by the proximity of a carbonyl group thereby permitting β-hydrogen rearrangement. The rearranged hydrogen becomes attached to the carbonyl oxygen of the adjacent monomer unit. Consequently the hydrogen rearrangement leads to the selective cleavage at the –O–CH– linkage between the two monomer units in the macromolecule.

Valuable supplementary information about the mechanism of fragmentation can be provided by theoretical analysis through calculation of the dissociation rate constants based on quantum chemical studies of the potential energy surface, vibrational analysis and dynamical simulations of fragmentation events [27–33]. Application of computational quantum chemistry is mainly limited by the size of the species studied. In MS^n experiments one deals with the bond breaking and forming processes. Such processes are commonly studied with the density functional theory (DFT) [34–37,40–42] [38,39] which accounts for a degree of correlation among the electrons.

Here we report that first-principles DFT exploration of the ground state potential energy surface of $[PHB_n\text{-}H]^-$ identifies an alternative fragmentation channel to the hydrogen-rearrangement mechanism described above. Moreover, our calculations suggests that this alternative channel, a direct fragmentation pathway, is the energetically favored one. According to the statistical RRKM theory, this should be the main dissociation mechanism. By contrast, the MS^n experiments give evidence that another mechanism, which leads to appearance of larger fragments, is the dominant one. To understand this discordance, we have carried out molecular dynamics (MD) simulations of dissociation events. From these dynamical simulations it can be concluded that the fragmentations observed at low collision energy favor the direct fragmentation channel and are more closely modeled as a thermal fragmentation process. By contrast, fragmentations observed at higher collision energy favor the indirect fragmentation channels and are more closely modeled as a fast CID process.

Previous preliminary studies [43] employing density functional theory dealt only with geometry optimization of the transition state (TS) for an indirect fragmentation process, namely that for proton transfer from the methylene group of $[PHB_2\text{-}H]^-$. Because dynamical simulations based on DFT are computationally intractable given the size of these oligomeric species, an important ancillary goal of this paper is identification of appropriate theoretical models that are less computationally expensive, but which lead to a qualitatively acceptable description of the processes investigated here. Application of semi-empirical methods to the description of dissociation processes requires extra care because such methods can fail in the description of bond breaking and forming processes. For instance, recently in Ref. [44] the failure of commonly used semi-empirical methods to correctly describe acid dissociation has been discussed. Therefore, in this work the usefulness and accuracy of the semi-empirical AM1 [45] method is tested by comparison with the density functional theory (DFT) studies of fragmentation mechanisms. With knowledge of the limits of accuracy based on this comparison, we report the molecular dynamic studies of collision-induced and thermal dissociation processes at the semi-empirical AM1 level of theory.

2. Experimental details

Electrospray mass spectrometry analysis (ESI-MS^n) of poly(R,S)-3-hydroxybutyrate, which contains crotonate and carboxyl end groups, was performed using a Finnigan LCQ ion trap mass spectrometer (Finnigan, San Jose, CA, USA). Samples of the polyester were dissolved in methanol and the solutions introduced to the ESI source by continuous infusion at a rate of 3 μL/min using the instrument syringe pump. The LCQ ESI source was operated at 4.5 kV and the capillary heater set to 200 °C. Nitrogen was used as the nebulizing gas. For ESI-MS/MS experiments, the ions of interest were isolated monoisotopically in the ion trap and collisionally activated. The helium damping gas present in the mass analyzer served also as the collision gas. The RF amplitude was set to a value that caused the peak height of the precursor ion to decrease by at least 50%. The analysis was performed in negative ion mode.

To obtain some insight into the collision energy dependence of the fragmentation, experiments were also carried out in which fragment ion abundances were measured as function of RF amplitude. In the presentation of these cases, energy is reported in percent, where 100% corresponds to 5 V peak-to-peak RF excitation voltage.

3. Computational methodology and details

In the present investigation, several theoretical tools have been applied to study the fragmentation of PHB anions in the series of $[PHB]_n^-$ oligomers up to pentamers. These studies include: first-principles (DFT) explorations of the potential energy surfaces (PES) for selected species, RRKM calculations of dissociation rates for activated precursor ions, and MD simulations of thermal dissociation and CID based on the AM1 potential energy surface.

Exploration of the potential energy surfaces was performed by carrying out geometry optimization at several points, including; the reactants, products and transition states for fragmentation. Following optimization, stationary points were confirmed with local curvature checks, i.e. by confirming the presence of the correct number of positive real eigenvalues of the Hessian matrix. Transition state optimizations were also followed-up by intrinsic reaction coordinate analysis in both directions to verify that TS found connects the appropriate reactant and product under consideration. The DFT calculations were performed with the popular B3LYP [46] functional. For the dimer $[PHB]_2^-$, calculations were carried out using the 6-311G(p,d) basis set [47–52]. Stationary points for larger PHB species were determined using the 6-31G(d,p) [47–53] basis set, but an otherwise identical procedure. (Note that initially, for the dimer, we used the unrestricted HF scheme, seeing it as more suitable to model bond-breaking and -forming processes. During the course of the investigations it was observed that the DFT/RB3LYP/6-311(d,p) level of theory leads to results identical to DFT/UB3LYP/6-311(d,p) for $[PHB_2\text{-}H]^-$, so the spin-restricted

Table A1
Comparison of energies (in kcal/mol) at stationary points for the direct and indirect fragmentation processes of the dimer and tetramer anions at semi-empirical AM1 and DFT/B3LYP theory levels.

	AM1		DFT	
	Dimer	Tetramer	Dimer	Tetramer
Direct process				
Reactant	0	0	0	0
TS	37	35	18	17
Product (two neutral molecules)	13	9.2	−5.8	−5.1
Indirect process				
Reactant	0	0	0	0
TS	56	54	51	39
Product (one molecule)	8.1	5.5	7.6	7.6

scheme was used for the higher oligomers.) These studies of the ground-state potential energy surfaces were performed using the Gaussian 03 computer program [54].

Dissociation rate constants were calculated according to the statistical Rice–Ramsperger–Kassel–Marcus quasiequilibrium theory (RRKM/QET) using the direct count method as reported by Baer and Mayer [27].

In our MD simulations of CID we impact a single gas molecule with one immobile $[PHB_4\text{-}H]^-$ anion. The interaction potential for these MD simulations was taken to be that predicted by semi-empirical calculations with the AM1 parameterization [45]. In the experimental work, helium served as the collision gas, but since we lack semiempirical parameters for noble gases, for these simulations we have used the N_2 molecule with its principal axis aligned with the velocity vector to model the collision gas. In all cases the velocity vector of the collision gas molecule was targeted at the center of mass of $[PHB_4\text{-}H]^-$. The speed of the N_2 molecule was taken as a parameter in the simulations and ranged from 70 to 200 Å/ps. The time step was set to 0.001 ps, simulation time to 1 ps and the SCF convergence criteria was chosen as 0.0001. An ensemble of collision orientations was generated by rotating the target ion and using different conformations of the PHB tetramer anion. The molecular dynamics studies of CID were performed using HyperChem [55].

Knowing that semi-empirical methods frequently fail in description of bond breaking and forming processes, [44] we have examined the applicability of the semi-empirical AM1 method for the description of $[PHB_n\text{-}H]^-$ fragmentation. To do so, we compare the predictions of AM1 for barrier heights, bonds strengths and vibrational frequencies to predictions of the same with DFT calculations. Results of these comparisons are presented in the Appendix A and can be summarized as follows: All AM1 results are in qualitative accordance with the corresponding results of DFT calculations. Specifically, AM1 predicts the same relative ordering of the heights of barriers to fragmentation as computations at the higher theory level, but significant quantitative differences in the barrier height are present. A comparison of bond strengths and vibrational frequencies similarly confirms the qualitative reliability of AM1 for bond dissociation and the shape of the potential energy surface in the vicinity of minima, respectively. (See Table A1.) Based on these comparisons, we judge the semi-empirical AM1 method to be qualitatively acceptable for ranking fragmentation processes by energetic preference.

4. Results and discussion

4.1. Structure of the precursor ion

We start our studies with analysis of the initial ionization process in order to determine the probable molecular structure of $[PHB_n\text{-}H]^-$. For this purpose we have compared heights of the energy barriers to deprotonation for isomers of $[PHB_n]$, as calculated with DFT for dimers and tetramers. As expected, the most easily removable proton is that in the COOH moiety at the carboxylic end. The only other stable deprotonated structures that were identified resulted from the removal of a proton from the monomer unit at the opposite end of the molecule from the carboxylic acid group. In the dimer(tetramer) the energy cost of removing a proton from the $-CH_3$ group of this terminal monomer is 15.3(15.7) kcal/mole greater than that of removing the carboxylic proton. For both species, the energy cost of removing the methine proton is even greater. Based on these results, in the following we will limit ourselves to consider only carboxylate ($R\text{-}COO^-$) starting structures.

4.2. Dimer fragmentation

Having determined the most probable molecular structures of the $[PHB_2\text{-}H]^-$ precursor anions we proceed with a detailed analysis of the fragmentation pathways of the dimer anion $[PHB_2\text{-}H]^-$ ($m/z = 171$). The experimental MS/MS fragmentation spectrum for $[PHB_2\text{-}H]^-$ is presented in Fig. 1a [43].

The dimer fragmentation spectrum consists of two signals; m/z 171 and 85, consistent with the precursor $[PHB_2\text{-}H]^-$ ion and a fragment formed by the loss of a neutral molecule of 86 Da. Four possible dissociation pathways consistent with the observed fragmentation pattern are readily identified and these are depicted schematically in Scheme 1(a–d).

The first path, (1a) consists of direct cleavage of both the O3–C3 bond (marked "A" in Scheme 1) and the terminal CO_2, (by breaking the bond marked "D" in Scheme 1) but without proton transfer. The atom numbering is defined in Fig. 2, which also shows the geome-

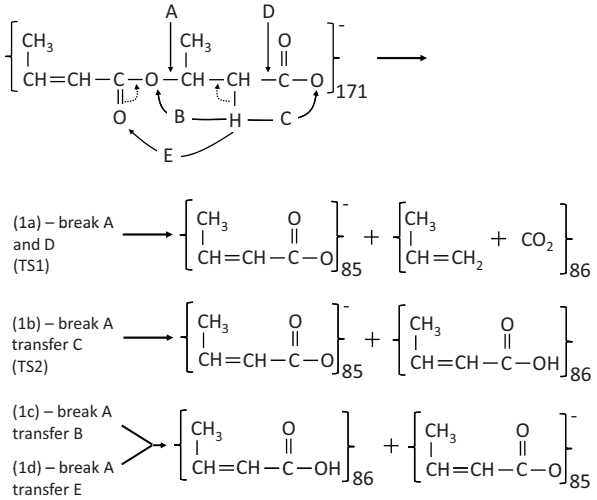

Scheme 1. Lettered arrows show possible locations of bond cleavage or proton transfer. Dotted arrows indicate electron rearrangement associated with mechanisms 1c and 1d.

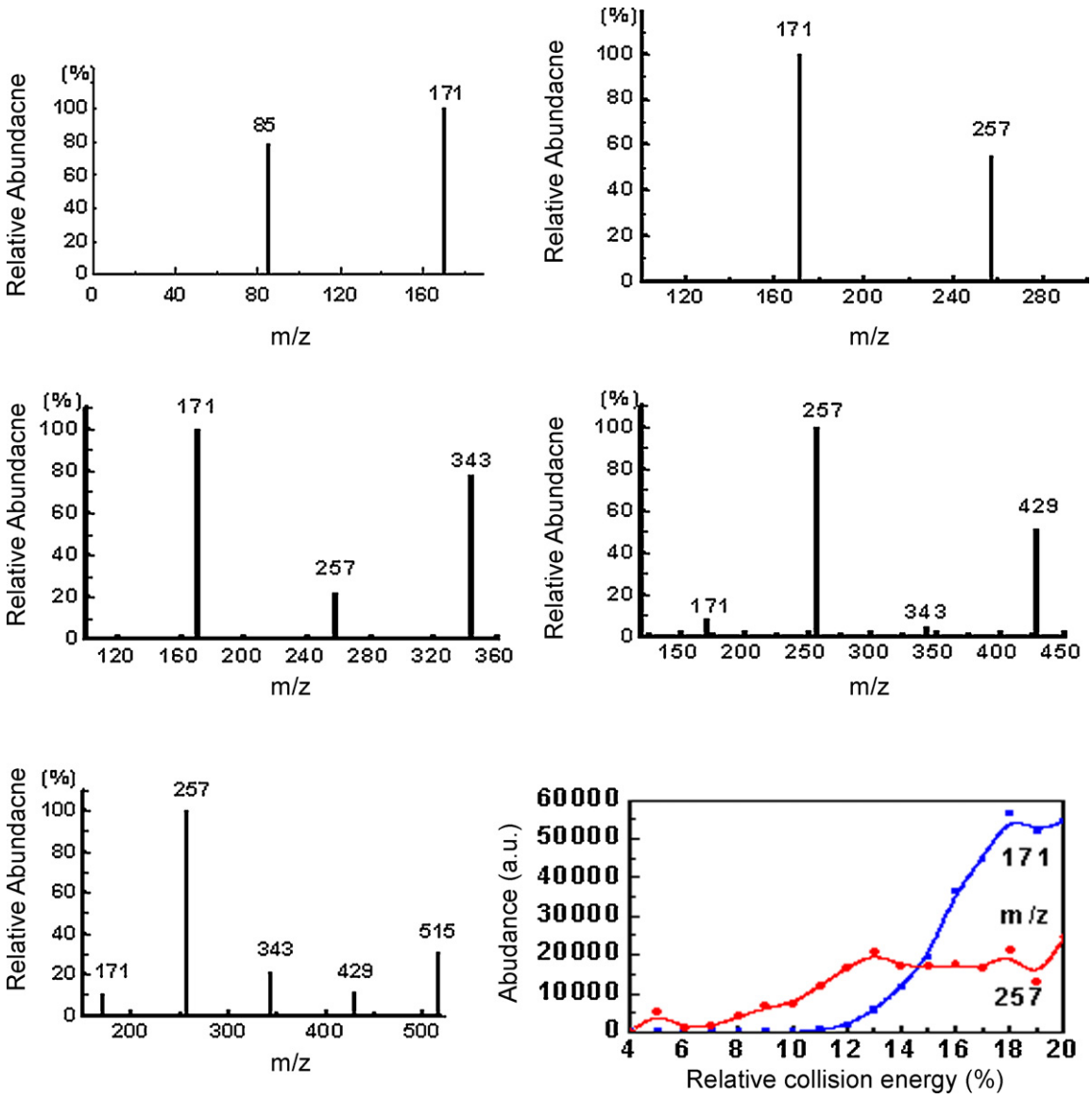

Fig. 1. ESI-MS/MS fragmentation spectrum (negative ion mode) obtained for selected $[PHB_n\text{-}H]^-$ precursor ions. Left to right, top to bottom: (a) $n = 2$ dimer, (b) $n = 3$ trimer, (c) $n = 4$ tetramer, (d) $n = 5$ pentamer, (e) $n = 6$ hexamer and (f) energy dependence of abundance of $m/z = 171$ & 257 fragment ions for the tetramer. The points are joined with splines as a visual aid.

try of the dimer optimized at the DFT/UB3LYP/6-311G(d,p) theory level.

The second process, (1b) is an indirect pathway for fragmentation considered by (some of) us previously [43]. This second process involves not only cleavage of the O3–C3 bond in $[PHB_2\text{-}H]^-$, but also intra-fragment proton rearrangement, nominally H1 transfer from C2 to O1 (marked "C" in Scheme 1). Paths 1c and 1d consist of cleavage of the O3–C3 bond in $[PHB_2\text{-}H]^-$ with *inter*-fragment proton transfer, through a 4-membered-ring structure ("B" in Scheme 1) in the case of 1c, and through a 6-membered-ring structure ("E" in Scheme 1) in the case of 1d. Path 1d is analogous to a McLafferty rearrangement.

First-principles exploration of the PES produced transition state structures consistent with paths 1a and 1b. No structures consistent with paths 1c and/or 1d were located. Fig. 3 shows the computationally predicted transition state geometries for fragmentation pathways (1a) and (1b).

Fig. 4 presents the potential energy profiles corresponding to minimum energy paths for 1a (through TS1) and 1b (through TS2), respectively. It is worth noting that direct cleavage of the C3–O3 bond leads to simultaneous elongation of the C1–C2 bond (Scheme 1a), while in the indirect fragmentation process (Scheme 1b) the C3–O3 bond length remains almost unchanged until the proton reaches its position for TS2 (from Fig. 3; d(C3–O3) = 2.11 Å and d(C1–C2) = 2.04 Å at TS1, whereas d(C3–O3) = 1.50 Å with d(C2–H1) = 1.49 Å at TS2). This comparison clearly shows that the direct fragmentation path is energetically more favorable. Not only is the barrier height for the direct dissociation pathway markedly lower in energy, (c.a. $\Delta E_1 = 18$ kcal/mol, vs. $\Delta E_2 = 51$ kcal/mol for the indirect pathway) but also the product energy for this fragmentation channel is lower. This finding suggests that fragmentation of $[PHB_2\text{-}H]$ anions occurs through the direct pathway, at least at low collision energies.

Our finding that the direct fragmentation path is energetically more favorable may seem counterintuitive because there are two stretched bonds at TS1 and only one at TS2, an observation suggesting that TS1 should be higher in energy. To clarify this apparent disagreement, we compare relative total energies, calculated for

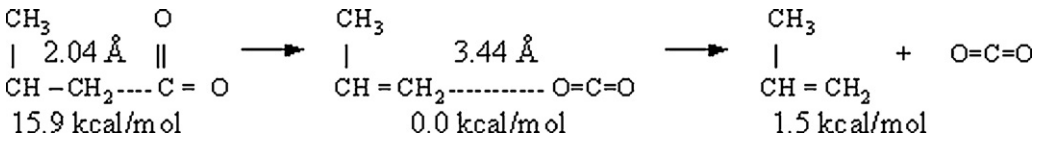

Scheme 2.

the neutral molecular system C_3H_6–CO_2 (86 Da), at two finite values of the C1–C2 distance between propene and carbon dioxide and additionally for infinite separation between them, as depicted in Scheme 2.

The computed energies were obtained from restrained geometry optimizations performed at the RB3LYP/6-31G(d,p) level for C1–C2 distances 2.04 Å, (corresponding to that at TS1) and 3.44 Å, (corresponding to that of the product for direct fragmentation channel of $[PHB_2\text{-}H]^-$). The last, (RHS) molecular configuration corresponds to infinite C1–C2 separation, for which the displayed relative energy is the sum of propane and carbon dioxide total energies. From these calculations it appears that energy the needed for cleavage of the C1–C2 bond is more than compensated for by formation of the double bond C2=C3 within propene and by strengthening of the bonds in the COO group as it relaxes into a carbon dioxide molecule, rendering the direct pathway energetically favored over the indirect one.

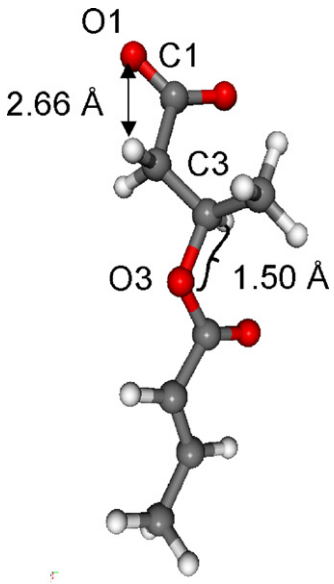

Fig. 2. Geometry of $[PHB_2\text{-}H]^-$ as optimized at the DFT/B3LYP/6-311G(d,p) theory level.

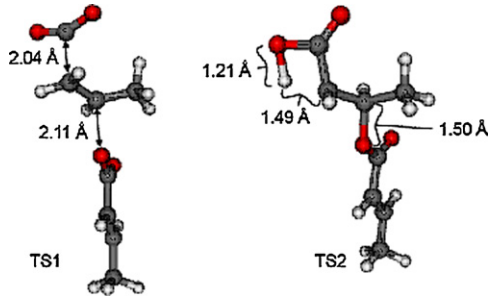

Fig. 3. Geometries at the transition states: TS1 – direct fragmentation (Scheme 1a) and TS2-fragmentation with the proton transfer (Scheme 1b) as optimized at the DFT/B3LYP/6-311G(d,p) theory level. Note the dramatic decrease in the O1-H distance in TS2 in comparison to the reactant structure in Fig. 2.

The experimental spectrum presented in Fig. 1a. gives little further insight into the dimer fragmentation mechanism because, in this simplest case, the alternative fragmentation pathways must lead to the same product masses. Therefore, to obtain more information it is necessary to study fragmentation of larger PHB oligomers both theoretically and experimentally. Fig. 1b–e shows the ESI-MS/MS fragmentation spectra of selected anions corresponding to PHB_n oligomers (from 3-mer to 6-mer) terminated by crotonic and carboxylic end groups. An examination of these spectra indicates that the most intense signals present in the ESI-MS/MS spectra correspond to product anions formed as a result of the loss of two or three 86 Da HB units from the selected molecular anion, with one exception, for trimers, which lose single 86 Da unit.

4.3. Trimer fragmentation

In the case of the trimer, cleavage of either of the –O–CH– linkages may results in two fragments, with m/z 171 and 85. The experimental fragmentation pattern for trimers (Fig. 1b) shows clearly that the lighter fragment always becomes neutral. Analogous to the case for dimers, four possible dissociation pathways consistent with the experimental fragmentation pattern are readily identified. These are shown in Scheme 3a–d. Again, the experimental spectrum does not give insight into which pathway is favored because all paths lead to product ions of the same mass.

4.4. Tetramer fragmentation

In contrast to the cases of the dimer and trimer, the experimental fragmentation spectrum of the tetramer does give some insight into which of the possible fragmentation pathways are physically operative. The dominant peak in the fragmentation pattern of the tetramer corresponds to loss of 172 = 2 × 86 Da units. This observation allows us to prune the list of possible fragmentation pathways.

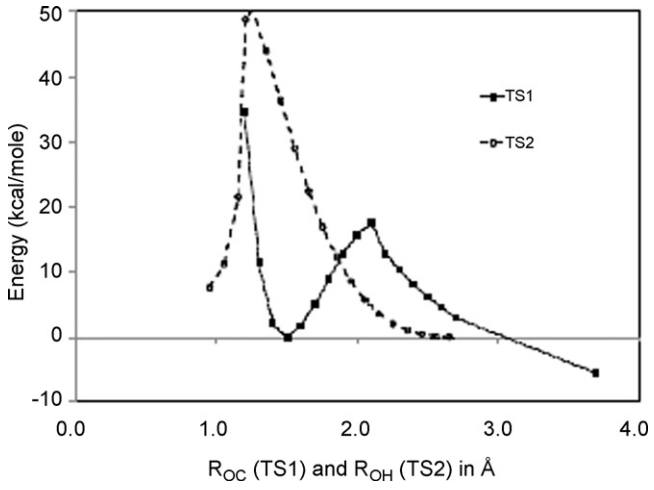

Fig. 4. Potential energy plots vs. distance $R_{(O3\text{–}C3)}$ and $R_{(H1\text{–}O1)}$, correspondingly for the direct (solid squares) and indirect (open circles) fragmentation pathways of the PHB^- dimer. The zero of energy is shifted to −384551.16 kcal/mol, corresponding to the reactant total energy. Adjacent points are joined by line segments as a visual aid.

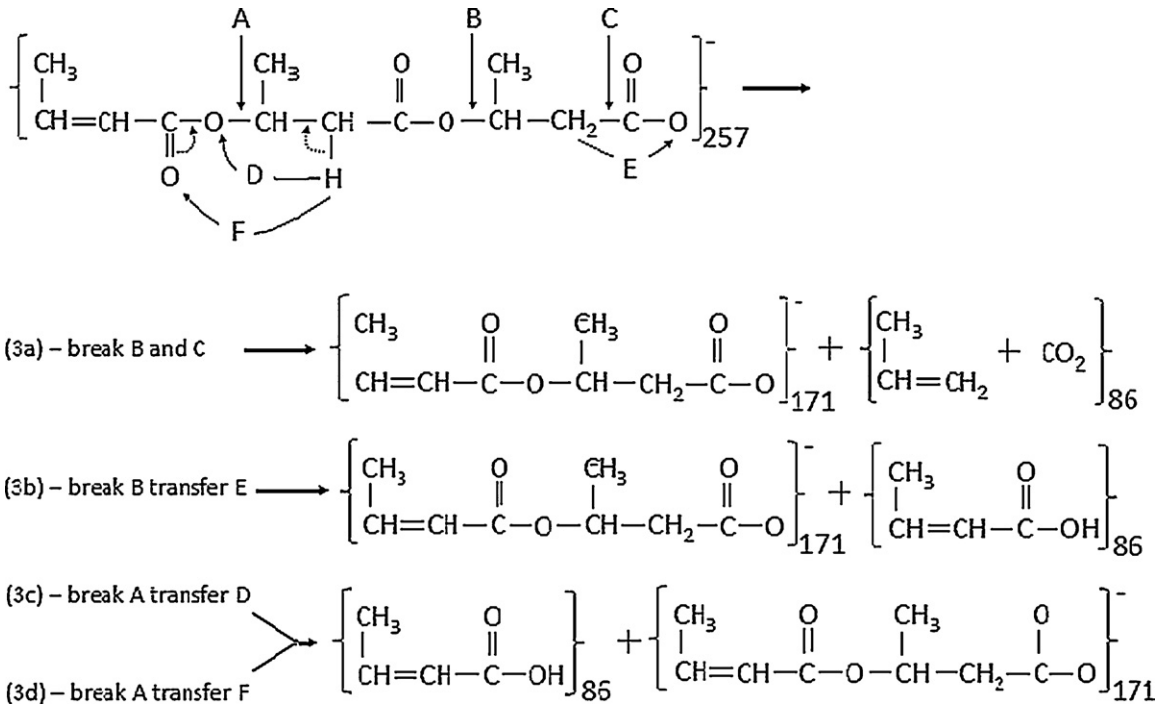

Scheme 3. Lettered arrows show possible locations of bond cleavage or proton transfer. Dotted arrows indicate electron rearrangement associated with mechanisms 3c and 3d.

For the tetramer, there are three –O–CH– linkages along the backbone. This opens up new fragmentation channels not available to the dimer or trimer. If fragmentation occurs at one of the two outer –O–CH– linkages, (marked "A" and "C" in Scheme 4) there are four possible dissociation pathways leading to an 86 Da neutral. These are shown in Scheme 4a–d and are analogous to those shown for dimers (Scheme 1a–d) and trimers (Scheme 3a–d). Specifically, loss of one single unit of mass 86 could result from direct fragmentation with loss of propene + carbon dioxide (4a), or from indirect fragmentation with either intra-fragment (4b) or inter-fragment (4c, 4d) hydrogen rearrangement. If the tetramer fragments at the interior –O–CH– linkage, (marked "B" in Scheme 4) however, two of the four corresponding dissociation pathways are exceedingly unlikely because they would lead to a carbon atom with unnatural valance, (sans some further hydrogen rearrangement, i.e. a statistically improbable double H-transfer). Pathway 4e would require hydrogen transfer (K) from the pentavalent carbon, (solid circle) to the trivalent carbon (dashed circle). Pathway 4f would require hydrogen transfer (L) to the trivalent carbon (dotted circle) from the adjacent CH_3. Only the H-transfer channels 4 g and 4 h appears to result in fragments that obey the rules of valance.

Further experimental characterization of the tetramer fragmentation shows that the fragmentation spectrum is collision energy dependent. In Fig. 1f, the relative abundances of $m/z = 171$ and $m/z = 257$ anions produced in the CID of tetramers are plotted as a function of RF excitation voltage. (RF is reported as a % of maximum, where maximum = 5 V peak-to-peak). While the ions in the MS trap are in the multiple collision regime and RF voltage does not equate to collision energy, collision energy should scale with applied RF voltage so higher RF potential implies more energetic collisions. The first trace of $m/z = 257$ signals appears at an applied RF voltage of ~5%. ($m/z = 257$ corresponds to loss of an 86 Da neutral.) With increasing collision energy, $m/z = 171$ anions appear at ~12% and rapidly increase in abundance, exceeding 257 ions at ~15% and heavily dominating at higher energies. ($m/z = 171$ corresponds to loss of a neutral of mass 172 Da, which is two 86 Da monomer units.) For reference, at 11% relative energy the attenuation of the precursor ions signal is <0.05 (For visual clarity the abundance of precursor ions is not displayed in Fig. 1f.).

We supplement these experimental data with theoretical analysis for the tetramer. First-principles explorations of the PES for the tetramer reveal transition state structures consistent with paths 4a (TS3) and 4 h (TS4). Path 4a is a direct fragmentation analogous to 1a for the dimer so TS3 for the tetramer is analogous to TS1 for the dimer. Path 4 h is an indirect one with inter-fragment hydrogen transfer. In contrast to the case of the dimer, for the tetramer the TS structure along the indirect path (TS4) includes a 6-membered ring structure, whereas for the dimer the TS structure along the indirect path (TS2) contains a 4-membered ring. Interestingly, no 6-membered-ring TS structure was identified for the dimer, even when the corresponding structure for the tetramer was used as a template to construct a starting structure for TS searching for the dimer. While failure to identify such a structure does not guarantee its absence, this finding does suggest that the dimer and tetramer TS structures for indirect fragmentation differ sufficiently that one cannot be used as a model for the other.

The optimized transition state geometries TS3 and TS4 are presented in Fig. 5. Relative energies for these TS structures, (referenced to the reactant energy) are compared in Table A1, where one can see that for tetramers the activation energy for the direct fragmentation is significantly lower then for an indirect dissociation, similar to the case of the dimer. Notice also that the activation energy for direct fragmentation of $[PHB_2\text{-}H]^-$ (18 kcal/mol) is almost the same as for $[PHB_4\text{-}H]^-$ (17 kcal/mol). This finding supports the hypothesis that there is a degree of transferability of the results for small oligomers to higher oligomers when the TS structures are qualitatively similar.

The theoretical analysis reported here for the dimer and tetramer reveals that the energetically more favorable fragmentation pathway is direct loss of an 86 Da neutral molecule as opposed to fragmentation with proton rearrangement. For a more quantitative comparison we have calculated the RRKM reaction rate constants for these fragmentations. The predicted reaction rate constants are: $4.5 \times 10^{13}\ s^{-1}$ and $6.3 \times 10^{6}\ s^{-1}$ for direct and indi-

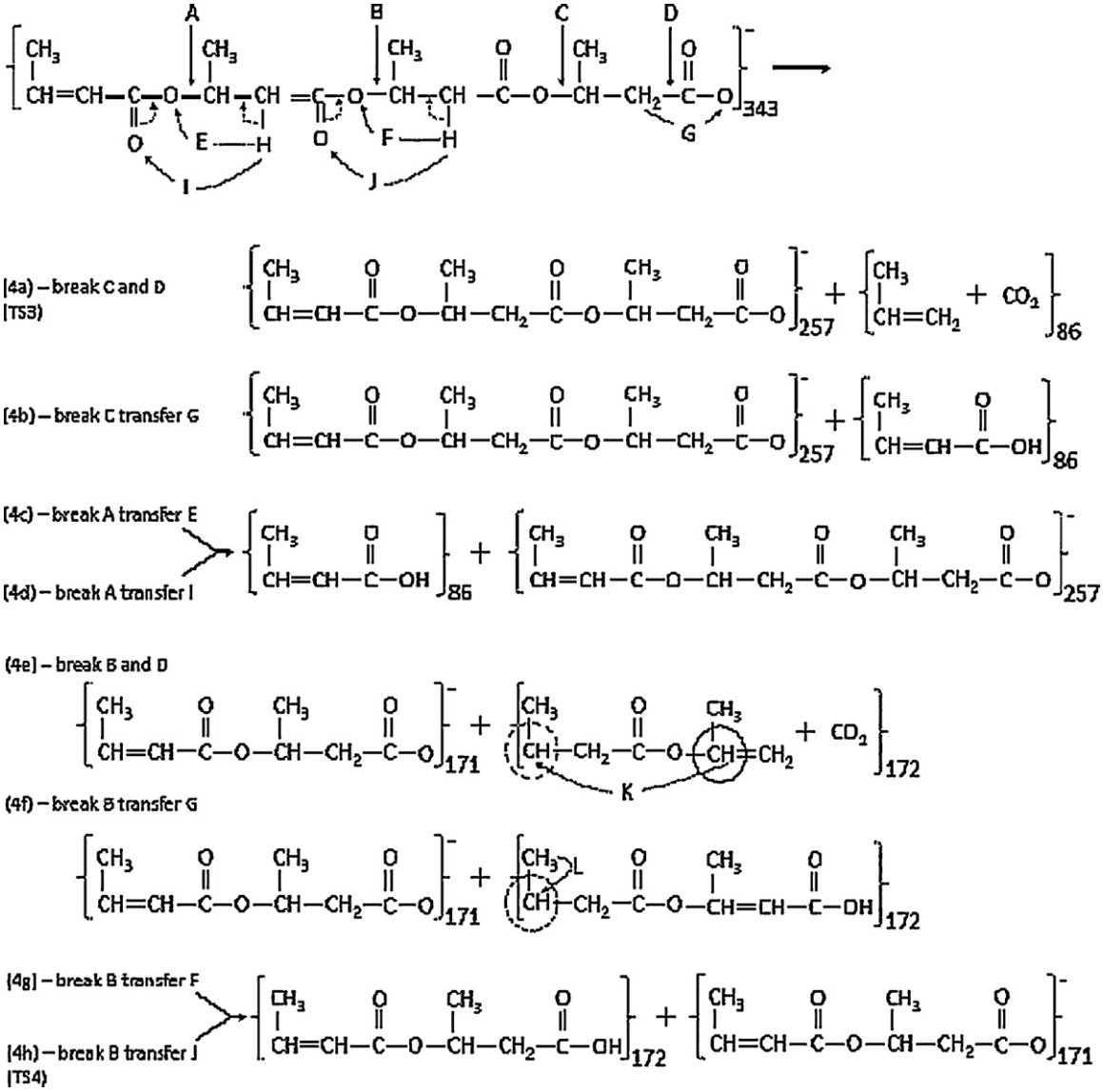

Scheme 4. Lettered arrows show possible locations of bond cleavage or proton transfer. Dotted arrows indicate electron rearrangement associated with mechanisms 4c, d, g and h.

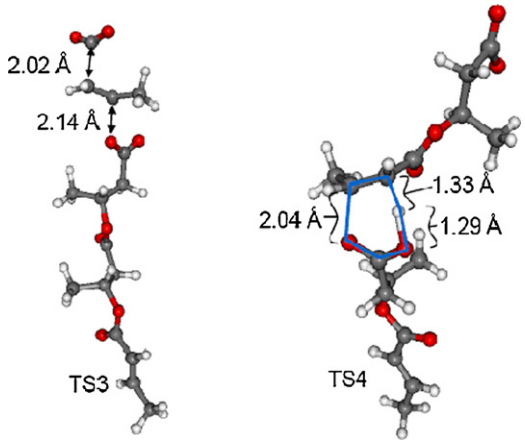

Fig. 5. Transition state geometries: TS3 – direct fragmentation and TS4 – fragmentation with the proton transfer, as optimized at the DFT/RB3LYP/6-31G(d,p) theory level. The 6-membered ring structure in TS4 is highlighted with the blue hexagon. Note the close resemblance of TS3 to TS1 in Fig. 3, while TS4 differs markedly from TS2.

rect dissociation of the dimer, respectively, and correspondingly $6.1 \times 10^{11}\ s^{-1}$ and $3.6 \times 10^{4}\ s^{-1}$ for the tetramer. As for the dimer, the direct fragmentation pathway is predicted to be dominant, and this is indeed the case near threshold collision energy, as shown in Fig. 1f. RRKM appears to break down, however, at higher collision energies. Similar behavior of RRKM is seen in the CID of CS_2 [56]. To analyze this phenomenon, we have performed molecular dynamics studies of CID processes for $[PHB_4\text{-}H]^-$ based on a semi-empirical (AM1) PES.

4.5. MD simulations

4.5.1. Simulations of CID

Molecular dynamics simulations were carried out for both thermal dissociation and CID processes. The MD simulations of CID exhibit both direct and indirect fragmentation processes. Four distinct regimes are apparent:

(i) For $v \leq v_{th}$ there is no fragmentation. Here v denotes the velocity of the N_2 molecule and v_{th} is a threshold velocity of ~115 Å/ps, (which corresponds to ~18 eV c.o.m. collision

energy) below which there is no fragmentation. Collisions in this regime may be inelastic in that they may result in some energy transfer, but no bond break or forming processes were observed (Video data CID_i.avi).

(ii) For $v > v_{th}$ up to $v = v_{th} + 20$ Å/ps, (~18–25 eV c.o.m.) some collisions result in the tetramer fragmenting into two dimers (d1 and d2; d1 with the COO end) with associated inter-fragment proton transfer. First, the corresponding OC bond breaks. Next the proton from the methyl group of d1 is transferred to neighboring O (of COO) in d2, which become neutral. These processes are akin to path 4 h in Scheme 4 (Video data CID_ii.avi).

(iii) For $v = v_{th} + 25$ Å/ps up to $v = v_{th} + 55$, (~26–39 eV c.o.m.) the same OC bond breaks as at lower collision energies, but the distance between the two dimers increases so quickly that *intra*-fragment proton rearrangement occurring within d1 appears as a mechanism. In this case d1 is neutral and d2 becomes the anion (Video data CID_iii.avi).

(iv) For $v > v_{th} + 55$ Å/ps, is as for $v > v_{th} + 25$ Å/ps, except other mechanisms appear. For example, d1 or d2 may fragment further by direct pathways (by loss of CO_2 and propane) (Video data CID_iv.avi).

At all collision velocities investigated in the simulations reported here, the N_2 molecule remains intact. No chemical reaction with the collision gas is observed.

The above velocity bounds are approximate and should not be taken as definite quantities. These bounds were seen to depend somewhat on the collision orientation, but in general the above four regimes remain qualitatively unchanged. A central observation from these simulations is that for moderate kinetic energy, two fragments appears (d1 and d2) and almost always the proton from the methyl group of d1 undergoes inter-fragment transfer to a neighboring O (of COO) in d2.

4.5.2. Simulations of thermal dissociation

The MD simulations of CID appear to be giving results opposite to the DFT explorations of the PES in the following respect: The DFT studies find that for both the dimer and the tetramer, the direct channel has a much lower TS barrier than the indirect channel. In fact, the energy barrier to the direct channel is so much lower that the indirect channel should not be observed at all at low collision energies. By contrast, in the MD simulations of CID, the first fragmentation mechanism to appear as the N_2 velocity is increased is an indirect one. (Seen in CID_ii.avi). Direct fragmentations only appear at higher collision velocities. The resolution of this apparent discrepancy lies in considering the conditions in the ion trap in the collision experiments.

In the ion trap, the damping/collision gas pressure is sufficiently high that the ions are in the multiple collision regime [57]. An ion undergoes 10 s to 100 s of collisions, each imparting a little internal energy to the ion, until it finally fragments. This building up of the internal energy in the ion little-by-little in many successive collisions is akin to a heating process. We have therefore carried out MD simulations of thermal dissociation. An example trajectory is shown in Thermal.avi, which shows thermal fragmentation of the tetramer at 3300 K. (The very high temperature was used to speed up the kinetics so that a dissociation event could be captured in a video of reasonable length.) (Video data Thermal.avi).

Unlike the simulations of CID, in thermal dissociation we find that the first dissociation process to appear with increasing temperature is the direct one.

In summary, the MD simulations of thermal fragmentation are completely consistent with the DFT explorations of the PES: The lowest energy fragmentation process is by the direct channel. This channel leads to the loss of a neutral of mass 86 Da, which is the first to appear with increasing energy in the energy-dependent fragmentation experiments, and is the first to appear upon increasing temperature in the MD simulations of thermal fragmentation.

In the energy-dependent fragmentation experiments, ions that most plausibly come from an indirect fragmentation process appear at higher energies, and rapidly become dominant with further increase in energy. Since the direct process is energetically favored, this dominance of the higher-energy indirect process at higher collision energies shows that the indirect process is statistically favored. This result is fully consistent with the MD simulations of CID, which show fragmentation by an indirect process with H-transfer.

4.6. Pentamer and hexamer fragmentation

For brevity, for the pentamer and hexamer species we do not provide schemes showing possible direct and indirect fragmentation paths. We do note, however, that no qualitatively new paths are expected. The plausible fragmentation pathways are analogous to those seen for the tetramer: loss of a terminal unit of mass 86 Da by direct or indirect fragmentation, and loss of two or more monomers by indirect fragmentation.

Experimental spectra for fragmentation of pentamers and hexamers are given in Fig. 1d and e, respectively. A strong signal at $m/z = 257$, corresponding to loss of $172 = 2 \times 86$ Da, dominates the pentamer fragmentation spectrum. For the hexamer, the dominant signal is again at $m/z = 257$, where it corresponds to loss of $258 = 3 \times 86$ Da. From these results, and by comparison to the tetramer, it is reasonable to surmise that these larger oligomers are predominantly fragmenting in the trap by an indirect mechanism involving proton transfer through a six-membered TS that leads to cleavage of an interior –O–CH– linkage. The lower intensity signals due to loss of an 86 Da neutral could plausibly arise from either direct or indirect fragmentation at a terminal –O–CH– linkage.

4.6.1. Conclusions

We have performed first-principles studies of the potential energy profiles for the fragmentation of poly[(R, S)-3-hydroxybutanoic acid] $[PHB_n\text{-H}]^-$ anions (up through tetramers) by both direct, and proton rearrangement, mechanisms. Subsequent statistical RRKM analysis of these processes indicates that fragmentation should proceed mainly through successive direct loss of a neutral of 86 Da. In contrast, experimental ESI MS/MS experiments show that $[PHB_n\text{-H}]^-$ ($n > 3$) dissociate by loss of larger fragments, suggesting that proton rearrangement dominates the fragmentation mechanism. This experimental finding is consistent with reports in the literature, which favor a proton-rearrangement mechanism. This apparent discordance is resolved with molecular dynamics simulations based on a semiempirical PES. Analysis of the results reveals that dissociation at low collision energy is more closely modeled as a thermal dissociation process. At higher collision energies, the proton rearrangement mechanism is favored, although direct loss of an 86 Da neutral, while not dominant, remains an active fragmentation channel.

Acknowledgements

K.S. thanks Y. Chen of the Fox Chase Cancer Research Center for valuable discussions about fragmentation mechanisms, and K.G. Owens for discussions about ion traps. H.B., G.A. and M.K. acknowledge financial support by the 7FPEU project “Animpol”, contract No. FP7-KBBE-2009-3-245084.

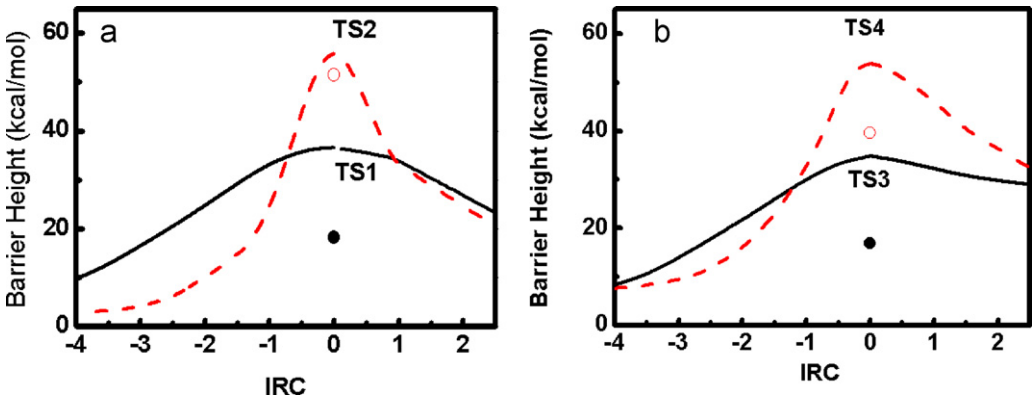

Fig. A1. Fragmentation paths along the intrinsic reaction coordinates for the direct (solid lines and cycles) and indirect processes (dashed curves and open circles). The curves are calculated using semi-empirical AM1 theory, while the points are calculated using DFT/B3LYP. The a and b panels present results for the dimer and tetramer of PHB anions, respectively. The zero of energy is set to the reactant total energy in all cases.

Appendix A.

To test the accuracy of the semi-empirical AM1 method for studies of PHB^- dissociation, we carried out calculations for the dimers and tetramers. First, calculated the reaction paths calculated within the intrinsic reaction path approach (IRC) at the AM1 level of theory and compared the barrier heights to the single-point DFT calculations. The results are presented in Fig. A1a and b for the dimer and tetramer respectively. The results show that while the quantitative barrier heights are markedly higher at the AM1 level, AM1 produces the same qualitative ordering of barrier heights as DFT.

Further numerical comparison is given in Table A1. As can be seen, AM1 significantly overestimates barrier heights relative to DFT, but it is also important to note that stationary points of the potential energy surfaces have one to one correspondences and the PES calculated at AM1 is free of artifacts (i.e. extraneous maxima and/or minima). Moreover, with AM1 one finds the same qualitatively fragmentation scenario as with DFT. Consequently, the RRKM quasi equilibrium theory with data from either semi-empirical AM1 theory or DFT will predict that direct fragmentations (black color lines) should be dominant. Additionally, in the Table A2. we have compared other important characteristic quantities: values of the imaginary frequencies and bond lengths at these transition states. Based on these data we judge that the semi-empirical (AM1) approach describes the fragmentation of the poly[(R, S)-3-hydroxybutanoic acid] $(PHB_n\text{-}H)^-$ anions qualitatively correctly. Therefore, we conclude this discussion that this methodology can be used in simulations of the collision induced dissociation processes with the purpose to gain qualitative insights.

Table A2
Comparison of values of characteristic parameters calculated for the dimer and tetramer anios at the corresponding transition states at semi-empirical AM1 and DFT/B3LYP theory levels. Frequencies in the units of cm^{-1} and bond distances in angstroms. ($i = \sqrt{-1}$).

	AM1		DFT	
	Dimer	Tetramer	Dimer	Tetramer
Direct				
ν	428 i	489 i	226 i	200 i
C3–O3	2.04	2.03	2.11	2.14
C1–C2	2.02	2.00	2.04	2.02
Indirect				
ν	2097i	1270i	1654i	1298i
O–C	1.48	1.67	1.44	2.04
H1–C1	1.49	1.54	1.49	1.33
O1–H1	1.33	1.12	1.21	1.29

Appendix B. Supplementary data

Supplementary data associated with this article can be found, in the online version, at doi:10.1016/j.ijms.2011.03.001.

References

[1] S. Naik, S.K.V. Gopal, P. Somal, World J. Microbiol. Biotechnol. 24 (2008) 2307.
[2] Y. Doi, Microbial Polyesters, VCH, New York, 1990.
[3] K. Sudesh, Y. Doi, Polym. Adv. Technol. 11 (2000) 865.
[4] G.Q. Chen, J. Biotechnol. 136 (2008) S286.
[5] H.E Valentin, D.L. Broyles, L.A. Casagrande, S.M. Colburn, W.L. Creely, P.A. DeLaquil, H.M. Felton, K.A. Gonzalez, K.L. Houmiel, K. Lutke, D.A. Mahadeo, T.A. Mitsky, S.R. Padgette, S.E. Reiser, S. Slater, D.M. Stark, R.T. Stock, D.A. Stone, N.B. Taylor, G.M. Thorne, M. Tran, K.J. Gruys, Int. J. Biol. Macromol. 25 (June–July (1–3)) (1999) 303.
[6] A.J. Anderson, E.A. Daves, Microb. Rev. 54 (1990) 450.
[7] Z. Jedliński, M. Kowalczuk, P. Kurcok, G. Adamus, A. Matuszowicz, W. Sikorska, R.A. Gross, J. Xu, R.W. Lenz, Macromolecules 29 (1996) 3773.
[8] S. Das, P. Kurcok, Z. Jedliński, R.N. Reusch, Macromolecules 32 (1999) 8781.
[9] M.W.F. Nielen, Mass Spectrom. Rev. 18 (1999) 309.
[10] G. Montaudo, R.P. Lattimer, Mass Spectrometry of Polymers Eds., Press, Boca Raton C.R.C.F.L., 2002.
[11] P.M. Peacock, C.N. McEwen, Anal. Chem 78 (2006) 3957.
[12] G. Montaudo, F. Samperi, M.S. Montaudo, Prog. Polym. Sci. 31 (2006) 277.
[13] E. Zagar, A. Krzan, G. Adamus, M. Kowalczuk, Biomacromolecules 7 (2006) 2220.
[14] Z. Jedliński, G. Adamus, M. Kowalczuk, R. Schubert, Z. Szewczuk, P. Stefanowicz, Rapid Commun. Mass Spectrom. 12 (1998) 357.
[15] G. Adamus, M. Kowalczuk, Rapid Commun. Mass Spectrom. 14 (2000) 195.
[16] A.H. Arkin, B. Hazer, G. Adamus, M. Kowalczuk, Z. Jedliński, R.W. Lenz, Biomacromolecules 2 (3) (2001) 623.
[17] G. Adamus, W. Sikorska, M.S. Montaudo, M. Scandola, M. Kowalczuk, Macromolecules 33 (2000) 5797.
[18] G. Adamus, W. Sikorska, M. Kowalczuk, I. Noda, M.M. Satkowski, Rapid Commun. Mass Spectrom. 17 (2003) 2260.
[19] G. Adamus, S.M. Montaudo, G. Montaudo, M. Kowalczuk, Rapid Commun. Mass Spectrom. 18 (2004) 1436.
[20] O. Laine, T. Laitnen, P. Vainiotalo, Rapid Commun. Mass Spectrom. 74 (2002) 4250;
S. Koster, M.C. Duursma, J.J. Boon, M.W.F. Nielen, C.G. Koster, R.M.A. Heeren, J. Mass Spectrom. 35 (2000) 739.
[21] M.A. Arnould, C. Wesdemiotis, R.J. Geiger, M.E. Park, R.W. Buehner, D. Vanderorst, Prog. Org. Coat. 45 (2002) 305.
[22] M.A. Arnould, R. Vargas, R.W. Buehner, C. Wesdemiotis, Eur. J. Mass Spectrom. 11 (2005) 243.
[23] P. Rizzarelli, C. Puglisi, G. Montaudo, Rapid Commun. Mass Spectrom. 20 (2006) 1683.
[24] G. Adamus, Rapid Commun. Mass Spectrom. 21 (2007) 2477.
[25] G. Adamus, M. Kowalczuk, Biomacromolecules 9 (2008) 696.
[26] G. Adamus, Macromolecules 42 (2009) 4547.
[27] T. Baer, P.M. Mayer, J. Am. Soc. Mass Spectrom. 8 (1997) 103.
[28] D.G. Truhlar, C. Bruce, B.C. Garrett, S.J. Klippenstein, J. Phys. Chem. 100 (1996) 12771.
[29] J. Zheng, S. Zhang, B.J. Lynch, J.C. Corchado, Y.Y. Chuang, P.L. Fast, W.P. Hu, Y.P. Liu, G.C. Lynch, K.A. Nguyen, C.F. Jackels, A. Fernandez Ramos, B.A. Ellingson, V.S. Melissas, J. Villà, I. Rossi, E.L. Coitiño, J. Pu, T.V. Albu, R. Steckler, B.C. Garrett, A.D. Isaacson, D.G. Truhlar, POLYRATE-version 2008, University of Minnesota, Minneapolis, 2008.
[30] K. Park, K. Song, W.L. Hase, Int. J. Mass Spectrom. 265 (2007) 326.

[31] B. Paizs, S. Suhai, Rapid Commun. Mass Spectrom. 15 (2001) 651.
[32] R. Spezia, J.Y. Salpin, M.P. Gaigeot, W.L. Hase, K. Song, J. Phys. Chem. A 113 (2009) 13853.
[33] P.B. Armentrout, H. Koizumi, M. MacKenna, J. Phys. Chem. A 109 (2005) 11365.
[34] R.C. Nuwan Hallowita, P.B. Damon, M.T. Armentrout, J. Rodgers, Phys. Chem. A 112 (2008) 7996.
[35] J. Liu, B. Van Devener, S.L. Anderson, J. Chem. Phys. 116 (2002) 5530.
[36] A.K. Shukla, J.H. Futrell, J. Mass Spectrom. 35 (2000) 1069.
[37] W.H. Green, C.B. Moore Jr., W.F. Polik, Annu. Rev. Phys. Chem. 43 (1992) 591.
[38] B. Kanawati, M. Harir, P. Schmitt-Kopplin, Int. J. Mass Spectrom. 288 (2009) 6.
[39] S.Y. Kim, J.Ch. Choe, Int. J. Mass Spectrom 294 (2010) 40.
[40] W. Kohn, I.J. Sham, Phys. Rev. 140 (1965) A1133.
[41] D.H. Aue, M. Guidoni, L.D. Betowski, Int. J. Mass Spectrom. 201 (2000) 283.
[42] Y. Xu, C. Afonso, Y. Gimbert, F. Fournier, X. Dong, R. Wen, J.C. Tabet, Int. J. Mass Spectrom. 286 (2009) 43.
[43] H. Bednarski, G. Adamus, M. Kowalczuk, in: B. Dębska, G. Fic (Eds.), Information Systems in Chemistry, 2006, ISBN 83-7199-415-X, 13.
[44] O.I. Arillo-Flores, M.F. Ruiz-López, M.I. Bernal-Uruchurtu, Theor. Chem. Acc. 118 (2007) 425.
[45] M. Dewar, W. Thiel, J. Am. Chem. Soc. 99 (1977) 4499.
[46] A.D. Becke, J. Chem. Phys. 98 (1993) 5648.
[47] P.J. Stephens, F.J. Devlin, C.F. Chabalowski, M.J. Frisch, J. Phys. Chem. 98 (1994) 11623.
[48] A.D. MacLean, G.S. Chandler, J. Chem. Phys. 72 (1980) 650.
[49] R. Krishnan, J.S. Binkley, R. Seeger, J.A. Pople, J. Chem. Phys. 72 (1980) 650.
[50] R. Ditchfield, W.J. Hehre, J.A. Pople, J. Chem. Phys. 54 (1971) 724.
[51] W.J. Hehre, R. Ditchfield, J.A. Pople, J. Chem. Phys. 56 (1972) 2257.
[52] P.C. Hariharan, J.A. Pople, Theoret. Chim. Acta 28 (1973) 213.
[53] M.J.S. Dewar, E.G. Zoebish, E.F. Healy, J.J.P. Stewart, J. Am. Chem. Soc. 107 (1985) 3902.
[54] M.J. Frisch, G.W. Trucks, H.B. Schlegel, G.E. Scuseria, M.A. Robb, J.R. Cheeseman, J.A. Montgomery, T. Verven Jr., K.N. Kudin, J.C. Burant, J.M. Millam, S.S. Iyengar, J. Tomasi, V. Barone, B. Mennucci, M. Cossi, G. Scalmani, N. Rega, G.A. Petersson, H. Nakatsuji, M. Hada, M. Ehara, K. Toyota, R. Fukuda, J. Hasegawa, M. Ishida, T. Nakajima, Y. Honda, O. Kitao, H. Nakai, M. Klene, X. Li, J.E. Knox, H.P. Hratchian, V. Cross, J.B. Bakken, C. Adamo, J. Jaramillo, R. Gomperts, R.E. Stratmann, O. Yazyev, A.J. Austin, R. Cammi, C. Pomelli, J.W. Ochterski, P.Y. Ayala, K. Morokuma, G.A. Voth, P. Salvador, J.J. Dannenberg, G. Zakrzewski, S. Dapprich, A.D. Daniels, M.C. Strain, O. Farkas, D.K. Malick, A.D. Rabuck, K. Raghavachari, J.B. Foresman, J.V. Ortiz, Q. Cui, A.G. Baboul, S. Clifford, J. Cioslowski, B.B. Stefanov, G. Liu, A. Liashenko, P. Piskorz, I. Komaromi, R.L. Martin, D.J. Fox, T. Keith, M.A. Al-Laham, C.Y. Peng, A. Nanayakkara, M. Challacombe, P.M.W. Gill, B. Johnson, W. Chen, M.W. Wong, C. Gonzalez, J.A. Pople, Gaussian 03, Revision E.01, Gaussian, Inc., Wallingford, CT, 2005.
[55] HyperChem™, Hypercube, Inc., 1115 NW 4th Street, Gainesville, Florida 32601 USA.
[56] K. Sohlberg, Y. Chen, J. Chem. Phys. 101 (1994) 3831.
[57] D.E. Goeringer, D.C. Duckworth, S.A. McLuckey, J. Phys. Chem. A 105 (10) (2001) 1882–1889.